Analysis of Complementary RRAM Switching

Dirk J. Wouters, *Member, IEEE*, Leqi Zhang, Andrea Fantini, Robin Degraeve, Ludovic Goux, Yang Y. Chen, Bogdan Govoreanu, *Senior Member, IEEE*, Gouri S. Kar, Guido V. Groeseneken, *Fellow, IEEE*, and Malgorzata Jurczak

***Abstract*—A novel procedure to decompose the I–V switching curves of complementary resistive switching (CRS) RRAM cells into the intrinsic switching characteristics of its individual constituting elements is proposed based on the set behavior of HfO_2-based bipolar RRAM elements. Analysis of different types of complementary cells indicates that very similar intrinsic switching behaviors occur in strongly different types of bipolar switching RRAM, however with a strong material dependence of the characteristic switching voltage.**

***Index Terms*—Complementary resistive switch (CRS), memory devices, nonvolatile memory, resistive switching.**

I. Introduction

COMPLEMENTARY resistive switching (CRS) cells were first proposed in [1]. A CRS cell consists of two back-to-back-connected single resistive switching RAM (RRAM) elements. Interest for such CRS cells is driven by their strongly nonlinear I–V switching characteristics enabling application in selectorless dense RRAM cross-point arrays. The original CRS cell was built out of two metal-ion conducting bridging RAM (CBRAM) [2] elements. Since then, a variety of other CRS cells have been published based not only on CBRAM [3] but also on metal oxide [4], [5] and even on amorphous carbon [6] materials.

In this work, CRS cells are fabricated by stacking HfO_2-based RRAM elements [7]. Based on the intrinsic switching properties of a single element and analysis of the set process [8], a novel procedure for decomposition of the CRS cell I–V into the individual intrinsic switching characteristics of each of the two RRAM elements is proposed. In this, the switching states of the CRS cell as originally defined in [1], [3], and [6] are reconsidered. Furthermore, the same decomposition analysis is applied on different published cells, revealing very similar intrinsic switching behavior of different RRAM elements but with a characteristic switching voltage that is material system dependent, evidencing indirect findings in [9].

Manuscript received March 14, 2012; revised May 1, 2012; accepted May 4, 2012. Date of publication June 13, 2012; date of current version July 20, 2012. This work was supported in part by the industrial partners to imec's Industrial Affiliation Program on RRAM. The review of this letter was arranged by Editor D. Ha.

D. J. Wouters, L. Zhang, Y. Y. Chen, and G. V. Groeseneken are with imec, 3001 Leuven, Belgium, and also with the ESAT, KU Leuven, 3001 Leuven, Belgium. (e-mail: dirk.wouters@imec.be; leqi.zhang@imec.be; yangyin.chen@imec.be; Guido.Groeseneken@imec.be).

A. Fantini, R. Degraeve, L. Goux, B. Govoreanu, G. S. Kar, and M. Jurczak are with imec, 3001 Leuven, Belgium (e-mail: andrea.fantini@imec.be; robin.degraeve@imec.be; ludovic.goux@imec.be; govorean@imec.be; Gouri.Kar@imec.be; malgorzata.jurczak@imec.be).

Color versions of one or more of the figures in this letter are available online at http://ieeexplore.ieee.org.

Digital Object Identifier 10.1109/LED.2012.2198789

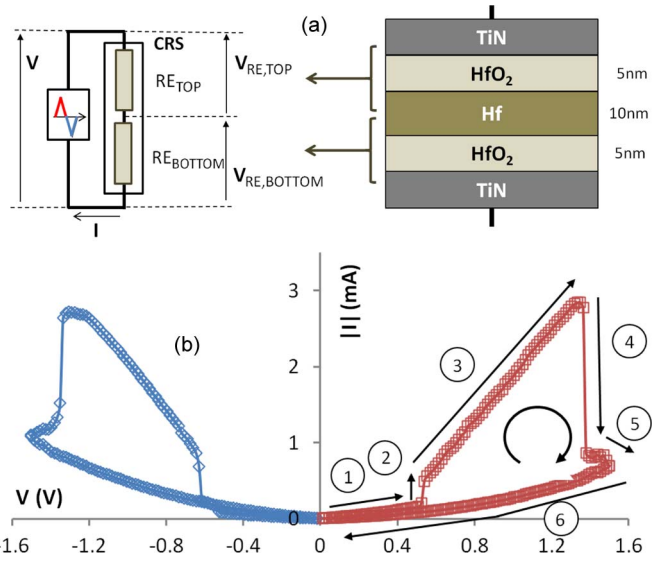

Fig. 1. (a) Schematic structure of experimental CRS cell. (b) Measured I–V switching characteristics of CRS (events numbered 1–6 correspond to Fig. 3).

II. Experiment

Our CRS cell structure consists of two back-to-back-stacked TiN \ HfO_2 \ Hf elements [Fig. 1(a)]. A 40-nm TiN bottom electrode (BE) was deposited on 300-mm Si wafers with physical vapor deposition (PVD). Subsequently, 5-nm HfO_2, 10-nm Hf, and another 5-nm HfO_2 were deposited. The HfO_2 was deposited by atomic layer deposition, and Hf was deposited by PVD. Finally, 30-nm PVD TiN was deposited as top electrode (TE). Then, the TiN TE and HfO_2 \ Hf \ HfO_2 stack was patterned by lithography and dry etching, stopping on the BE. Large test structures $(55 \times 55\ \mu m^2)$ were used allowing direct TE probing.

I–V characteristics were measured using a parameter analyzer (Agilent B1500A) and triangular voltage ramps (ramp rate $\sim$10 V/s). After forming, complementary-type characteristics were obtained [Fig. 1(b)]. (The main difference with the schematic curve [Fig. 2(b)] is a larger cell off-current.)

III. Decomposition Analysis of CRS

A. Intrinsic SET Process in HfO_2 RRAM

The intrinsic switching characteristics of single HfO_2\Hf RRAM elements were studied using special integrated

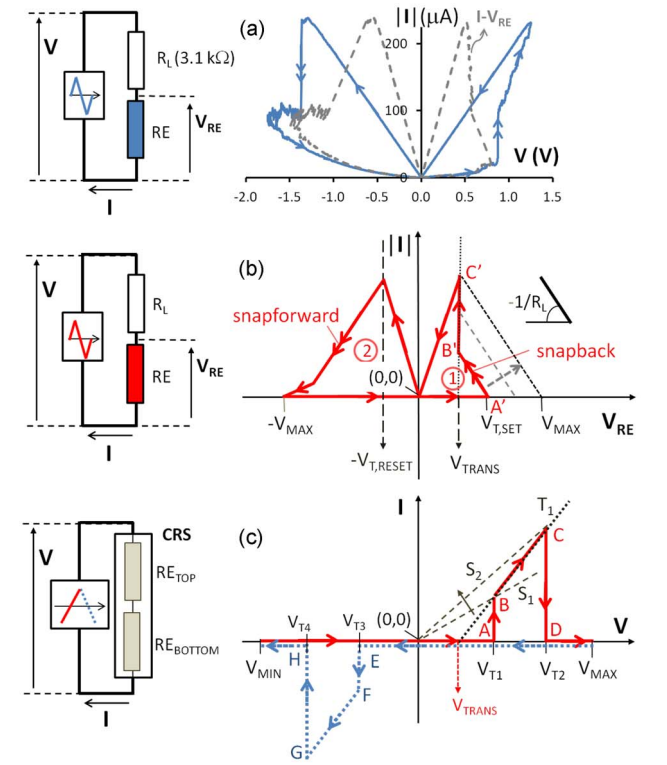

(d)	V_{MIN} to V_{T1}	V_{T1}	A-B	B-C	V_{T2}	C-D	D to V_{MAX}	V_{MAX} to V_{T3}	V_{T3}	E-F	F-G	V_{T4}	G-H	H to V_{MIN}
RE TOP	LRS	LRS	LRS	LRS	start reset	reset part 1	reset part 2	HRS	start set	set part 1	set part 2	LRS	LRS	LRS
RE BOTTOM	HRS	start set	set part 1	set part 2	LRS	LRS	LRS	LRS	LRS	LRS	LRS	start reset	reset part 1	reset part 2

Fig. 2. (a) (Solid curve) Measured I–V characteristic of a $HfO_2\backslash Hf$ RRAM element integrated with a 3.1-kΩ series resistance R_L [8]. The dashed curve gives the intrinsic I–$V_{\rm RE}$ curve by subtracting the voltage drop IR_L over the series resistor. (b) Schematic intrinsic switching characteristics I–$V_{\rm RE}$ of single RE. Starting from HRS: (1) Set starts at $V_{\rm RE} = V_{T,\rm SET}$ (point A'). The element resistance suddenly decreases, resulting in voltage snapback, until point B' following R_L load line. Set then continues at constant voltage $V_{\rm TRANS}$ until point C'. (2) Reset starts at $V_{T,\rm RESET} = -V_{\rm TRANS}$, followed by a rapid increase (*snapforward*) of $V_{\rm RE}$, and further gradual reset until reaching $-V_{\rm MAX}$ (assuming that $R_L \ll R_{HRS}$). (c) Schematic I–V switching curve of CRS cell. (d) Switching states of top and bottom REs during CRS I–V sweep. In all regions, (only) one of the elements is in LRS.

two-resistor (2R) test structures, with the RRAM element connected to a fully integrated resistive load R_L [Fig. 2(a)] [8]. The important observation of this work is that the set process occurs at a constant voltage, called the transition voltage $V_{\rm TRANS}$. In the first stage of the set [Fig. 2(b)], we observe a snapback of the voltage $V_{\rm RE}$ over the resistive element (RE) from the set trigger voltage $V_{T,\rm SET}$ to $V_{\rm TRANS}$. After the snapback, a further increase of the applied voltage increases the current through the element (following the shift of the load line), while the voltage over the element remains constant at $V_{\rm TRANS}$. Its *total* resistance further decreases (i.e., set continues) as $V_{\rm TRANS}/I$ (with $I = (V - V_{\rm TRANS})/R_L$), while its *differential* resistance $dR_{\rm RE} = dV_{\rm RE}/dI = 0$. When $V = V_{\rm MAX}$, the maximum current is reached (minimum $R_{\rm RE} = R_{\rm LRS}$), and reduction of V reduces $V_{\rm RE} < V_{\rm TRANS}$ stopping set and leaving $R_{\rm RE}$ constant at $R_{\rm LRS}$. $V_{\rm TRANS}$ was found to be independent of current range (up to > 200 μA) and logarithmically dependent on voltage sweep rate [8], but in the current experiments using limited sweep rates, this can, in the first order, be neglected. Note that this $V_{\rm TRANS}$ is equal to the indirectly derived set control voltage V_C in [9]. Furthermore, the low resistive state (LRS) resistance ($R_{\rm LRS}$) can be considered linear as long as maximal set current is at least a few tens of microamperes [8], which is the case in the current experiments.

B. Decomposition Procedure and Results

To reconstruct the individual memory element switching characteristics I–$V_{\rm RE,TOP}$ and I–$V_{\rm RE,BOTTOM}$ from the CRS cell I–V [schematic in Fig. 2(c)], we need to determine in each (I, V) point the resistance of the two (top and bottom) elements $R_{\rm TOP}(I, V)$ and $R_{\rm BOTTOM}(I, V)$. From that, we can calculate

$$V_{\rm RE,TOP/BOTTOM}(I, V) = IR_{\rm TOP/BOTTOM}(I, V). \quad (1)$$

For our HfO_2 CRS cell, set/reset of the bottom/top element occurs at positive voltages (to the TE), while reset/set of the bottom/top element occurs at negative voltages. Hence, the total I–V triangular sweep can be divided into two regions [Fig. 2(d)]: Between (the end of) positive set and (start of) negative reset, the bottom element is in LRS state, while between (the end of) negative set and (start of) positive reset, the top element is in LRS state. In each point, as we know the total resistance ($R_{\rm TOTAL} = V/I$), we can calculate the other resistance, e.g., in the first region

$$R_{\rm TOP}(I, V) = (R_{\rm TOTAL}(I, V) - R_{\rm LRS,BOTTOM} - R_{\rm SERIES}) \quad (2)$$

with $R_{\rm SERIES}$ as an additional (externally applied and/or internal parasitic) series resistance, assumed to be constant. Thus, the only issue remaining is the determination of the $R_{\rm LRS}$ of the two elements (and of $R_{\rm SERIES}$).

For that, we first argue that, in the CRS characteristics in Fig. 2(c), we can also discriminate, for each RE, the two stages of set, e.g., for the positive voltage swing, set of the bottom RE starts in point A but continues up to point C. Region A–B corresponds to the first (*snapback*) stage, while region B–C with constant slope corresponds to the second (*constant voltage*) stage. Indeed, it is observed that the extrapolated line T_1 tangent to region B–C does not cross the origin, proving that the *total* cell resistance still decreases from B to C (corresponding to the increase in slope of S_1 to S_2) and, thus, that set only stops in point C due to the start of reset of the top RE connected in series. Thus, refining the state analysis in [1], [3], and [6], only in the point C, both REs are in LRS

$$\frac{V(C)}{I(C)} = (R_{\rm TOP,LRS} + R_{\rm BOTTOM,LRS} + R_{\rm SERIES}). \quad (3)$$

On the other hand, as the second stage of set B–C occurs with zero differential resistance $dR_{\rm BOTTOM}$, we can calculate

$$Slope(T_1) = (dR_{\rm TOTAL})^{-1}\big|_{B-C} = (R_{\rm TOP,LRS} + 0 + R_{\rm SERIES})^{-1}. \quad (4)$$

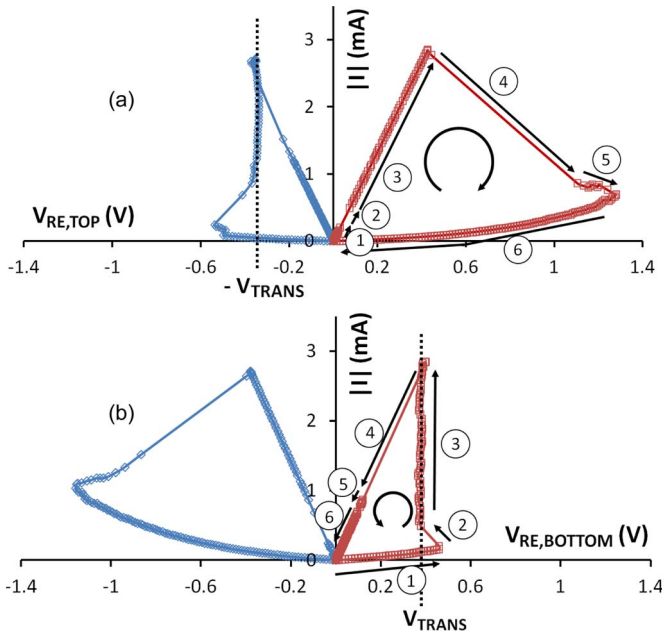

Fig. 3. Calculated I–V switching characteristics of (a) top and (b) bottom REs. For positive voltage swing, corresponding events are numbered 1–6: (1) Increase of V_{RE} until (2) first (*snapback*) part of set of bottom RE, (3) second part of set of bottom RE at constant voltage V_{TRANS}, (4) start of reset of top RE (*snapforward part*), (5) second part of reset of top RE, and (6) sweep back of applied voltage. Note that $I-V$ loop direction is opposite for bottom and top REs. Similar behavior is found for negative voltage swing, replacing top with bottom. Slight asymmetry may be due to different HfO_2 thicknesses.

TABLE I
PARAMETERS FOR DIFFERENT ANALYZED CRS CELLS

RRAM element	I_{max}	R_{LRS}[a]	R_{SERIES}	V_{TRANS}[b]	Ref
TiN\HfO$_2$\Hf\TiN	3 mA	~140 Ω	180 Ω	~0.36 V	-
Pt\SiO$_2$\GeSe\Cu	0.9 mA	~264 Ω	1050 Ω	~0.18 V	[1]
Pt\SiO$_2$\Cu	15 mA	~20 Ω	220 Ω	~0.26 V	[3]
Pt\Ta$_2$O$_{5-x}$\TaO$_{2-x}$\Pt	40 µA	~10 kΩ	44 kΩ	~0.40 V	[5]
Au\CNT\a-C\Au	80 µA	~24 kΩ	70 kΩ	~1.85 V	[6]

[a]Average for Top and Bottom RE; [b]Average of + and - V_{TRANS}

Thus, from (3) and (4) and from their equivalents for negative sweep, it is possible to calculate $R_{\mathrm{TOP,LRS}}$, $R_{\mathrm{BOTTOM,LRS}}$, and R_{SERIES}. From (2) (and equivalent), we can then determine $R_{\mathrm{TOP}}(I,V)$ and $R_{\mathrm{BOTTOM}}(I,V)$, and finally, from (1), we can determine the switching characteristics of each element. Based on this procedure, Fig. 3(a) and (b) shows the intrinsic switching curves derived from the CRS I–V given in Fig. 1(b) with the parameters listed in Table I. It can be seen that the obtained switching curves are very similar to that of the single element in the 2R experiment in Fig. 2(a) [8].

C. Comparison of Different CRS Cells

We applied the same analysis to CRS characteristics published in [1], [3], [5], and [6]. In all cases, we confirmed the decrease of R_{TOTAL} in the sloped regions between V_{T1} and V_{T2} (and V_{T3} and V_{T4}), indicating again a two-stage set, and the decomposition of the CRS I–V (although based on the set characteristics of a HfO_2 cell) gives very similar intrinsic switching curves as our cell. The different parameters are compared in Table I. While the actual R_{LRS} values scale well with the different current levels (and expected to be determined by the forming conditions), it is interesting to compare the V_{TRANS} values for the different cell types. The V_{TRANS} for our HfO_2 cell (~0.36 V), as well as that for the TaO_x cell in [5] (~0.40 V), compares well with the V_C of ~0.4 V in [9], while also the lower deduced V_{TRANS} for CBRAM cells (0.18–0.26 V) is in line with V_C of ~0.2 V for similar cells in [9]. It is interesting to see that carbon-based RRAM stacks increase V_{TRANS} to 1.85 V. While a dependence of V_{TRANS} on experimental conditions (as sample dimensions, etc.) cannot be excluded, the rather large differences observed suggest that V_{TRANS} is strongly correlated to the cell material.

IV. CONCLUSION

A novel procedure to decompose the switching curve of a CRS cell into the intrinsic switching curves of its two constituting antiserial connected REs has been proposed, based on the (set) switching characteristics of a single HfO_2 RE. Applying the same analysis on different types of CRS cells, although having strongly different operation physics, results in very similar intrinsic switching behavior, however with a constant set voltage parameter V_{TRANS} that is strongly depending on the cell material type.

REFERENCES

[1] E. Linn, R. Rosezin, C. Kügeler, and R. Waser, "Complementary resistive switches for passive nanocrossbar memories," *Nature Mater.*, vol. 9, no. 5, pp. 403–406, May 2010.
[2] M. Kund, G. Beitel, C.-U. Pinnow, T. Röhr, J. Schumann, R. Symanczyk, K.-D. Ufert, and G. Müller, "Conductive bridging RAM (CBRAM): An emerging non-volatile memory technology scalable to sub 20 nm," in *IEDM Tech. Dig.*, 2005, pp. 754–757.
[3] R. Rosezin, E. Linn, L. Nielen, C. Kügeler, R. Bruchhaus, and R. Waser, "Integrated complementary resistive switches for passive high-density nanocrossbar arrays," *IEEE Electron Device Lett.*, vol. 32, no. 2, pp. 191–193, Feb. 2011.
[4] J. Lee, J. Shin, D. Lee, W. Lee, S. Jung, M. Jo, J. Park, K. P. Biju, S. Kim, S. Park, and H. Hwang, "Diode-less nano-scale ZrO_x/HfO_x RRAM device with excellent switching uniformity and reliability for high-density cross-point memory applications," in *2011 IEDM Tech. Dig.*, pp. 19.5.1–19.5.4.
[5] M.-J. Lee, C. B. Lee, D. Lee, S. R. Lee, M. Chang, J. H. Hur, Y.-B. Kim, C.-J. Kim, D. H. Seo, S. Seo, U.-I. Chung, I.-K. Yoo, and K. Kim, "A fast, high-endurance and scalable non-volatile memory device made from asymmetric Ta_2O_{5-x}/TaO_{2-x} bilayer structures," *Nature Mater.*, vol. 10, no. 8, pp. 625–630, Jul. 2011.
[6] Y. Chai, Y. Wu, K. Takei, H.-Y. Chen, S. Yu, C. H. Chan, A. Javey, and H.-S. P. Wong, "Nanoscale bipolar and complementary resistive switching memory based on amorphous carbon," *IEEE Trans. Electron Devices*, vol. 58, no. 11, pp. 3933–3939, Nov. 2011.
[7] B. Govoreanu, G. S. Kar, Y.-Y. Chen, V. Paraschiv, S. Kubicek, A. Fantini, I. P. Radu, L. Goux, S. Clima, R. Degraeve, N. Jossart, O. Richard, T. Vandeweyer, K. Seo, P. Hendrickx, G. Pourtois, H. Bender, L. Altimime, D. J. Wouters, J. A. Kittl, and M. Jurczak, "10×10 nm^2 Hf/HfO_x cross-bar resistive ram with excellent performance, reliability and low-energy operation," in *IEDM Tech. Dig.*, 2011, pp. 31.6.1–31.6.4.
[8] A. Fantini, D. J. Wouters, R. Degraeve, L. Goux, L. Pantisano1, G. Kar, Y.-Y. Chen, B. Govoreanu, J. A. Kittl, L. Altimime, and M. Jurczak, "Intrinsic switching behavior in HfO_2 RRAM by fast electrical measurements on novel 2R test structures," in *Proc. 4th IEEE Int. Memory Workshop*, May 20–23, 2012, to be published.
[9] D. Ielmini, "Filamentary-switching model RRAM for time, energy and scaling projections," in *IEDM Tech. Dig.*, 2011, pp. 17.2.1–17.2.4.